Retrieval of aerosol microphysical properties using surface MultiFilter Rotating Shadowband Radiometer (MFRSR) data: Modeling and observations

Evgueni I. Kassianov, James C. Barnard, and Thomas P. Ackerman
Pacific Northwest National Laboratory, Richland, Washington, USA

Received 10 August 2004; revised 10 January 2005; accepted 2 February 2005; published 6 May 2005.

[1] MultiFilter Rotating Shadowband Radiometers (MFRSRs) are widely deployed over the world. These radiometers measure the total, direct, and diffuse components of shortwave, narrowband irradiance at six wavelengths. For five of these wavelengths, aerosol optical depths and single scattering albedos can be retrieved. We describe here a simple retrieval technique that can significantly extend the capability of the MFRSR to study atmospheric aerosols and can provide a means for simultaneous retrieval of the mean particle radius, total number of particles (for an assumed size distribution), and the imaginary refractive index. This technique is based on measurements of the direct irradiances at two wavelengths (0.415 μm and 0.870 μm) and the diffuse irradiance at 0.415 μm. Our technique requires assumptions regarding the shape of the aerosol size distribution, and the real part of the refractive index, as well as an estimate of the surface albedo at 0.415 μm. Given plausible values of these quantities, sensitivity tests show that successful retrievals of aerosol characteristics can be achieved. However, the retrieval does not work when the aerosol is dominated by coarse mode particles such as dust, because of the weak dependence of aerosol optical thickness on wavelength. The technique has been applied to derive time series of aerosol microphysical properties from MFRSR measurements taken during a single day, 27 April 2003, of the Mexico City Metropolitan Area field campaign. Additionally, MFRSR-derived aerosol properties are in good agreement with Aerosol Robotic Network (AERONET) retrievals made also in Mexico City.

Citation: Kassianov, E. I., J. C. Barnard, and T. P. Ackerman (2005), Retrieval of aerosol microphysical properties using surface MultiFilter Rotating Shadowband Radiometer (MFRSR) data: Modeling and observations, *J. Geophys. Res.*, *110*, D09201, doi:10.1029/2004JD005337.

1. Introduction

[2] Aerosol particles have a significant impact on the radiative and heat balance of the Earth-atmosphere system by absorbing and scattering solar radiation (direct aerosol effect) and altering cloud optical properties and suppressing precipitation (indirect aerosol effect) [e.g., *Haywood et al.*, 1997; *Russell et al.*, 1999; *Ramanathan et al.*, 2001a; *Yu et al.*, 2004]. However, significant uncertainties remain regarding the magnitude, and even the sign, of the aerosol forcing because of an incomplete knowledge of aerosol properties and their strong temporal and spatial variations [e.g., *Haywood and Boucher*, 2000; *Intergovernmental Panel on Climate Change* (*IPCC*), 2001]. Reduction of uncertainties in both the direct and the indirect aerosol effects requires accurate determination of the aerosol optical properties. The latter are functions of their microphysical characteristics, such as the aerosol shape, effective refractive index, and the aerosol size distribution.

0148-0227/05/2004JD005337$09.00

[3] Combined measurements of the direct normal solar irradiance and the angular distribution of the scattered solar radiation have been used successfully by the Aerosol Robotic Network (AERONET) program (http://aeronet.gsfc.nasa.gov/) [*Holben et al.*, 1998] to retrieve the aerosol microphysical characteristics [*Dubovik et al.*, 2002, and references therein]. Typically, observations of the direct irradiance and the angular distribution of sky radiances at four specific wavelengths (0.44, 0.67, 0.87, and 1.02 μm) are used for the aerosol retrievals. The latter give the columnar aerosol size distribution (from 0.1 to 7 μm) and the refractive index.

[4] Like the Sun photometer employed by AERONET, the Multifilter Rotating Shadowband Radiometer (MFRSR) [*Harrison et al.*, 1994] has been deployed worldwide. These radiometers provide measurements of the total and diffuse solar irradiances at six wavelengths (0.415, 0.5, 0.615, 0.673, 0.870, and 0.94 μm). Direct solar irradiances are obtained by differencing and the values are used to derive spectral values of the aerosol optical depth [e.g., *Harrison and Michalsky*, 1994; *Alexandrov et al.*, 2002], while single scattering albedos can be obtained from diffuse irradiances

[*Petters et al.*, 2003]. To further the utility of the MFRSR as an aerosol instrument, we propose here a simple retrieval technique that can extend the capability of the MFRSR by not only deriving the single scattering albedo (i.e., the imaginary part of the aerosol refractive index), but the aerosol size distribution as well. In a similar manner to *Petters et al.* [2003], we apply an iterative scheme to match the model results with observations; in contrast to *Petters et al.* [2003], we use separately both the direct and diffuse components of surface irradiance.

[5] The technique is described in section 2. In section 3, we estimate the accuracy of the proposed retrieval by using numerical experiments. Section 4 presents the results of applying this technique to actual MFRSR observations. In section 5, we discuss the assumptions of the retrieval. The main results are summarized in section 6.

2. Technique

[6] If we assume that aerosol particles are homogeneous spheres, then the Lorenz-Mie theory can be applied to relate the aerosol microphysical properties to aerosol optical properties [e.g., *van de Hulst*, 1981; *Bohren and Huffman*, 1998]. The equation for the height-dependent extinction coefficient $\sigma_\lambda(z)$ is

$$\sigma_\lambda(z) = \int_{a_{\min}}^{a_{\max}} \varphi(z,a) K_{e,\lambda}(a) da, \tag{1}$$

where $\varphi(z, a)$ denotes the aerosol size distribution as a function of height and a is the radius. The weighting function $K_{e,\lambda}(a)$ has the form

$$K_{e,\lambda}(a) = \pi a^2 Q_e(n, m; a/\lambda), \tag{2}$$

where Q_e is the extinction efficiency, n and m are the real and imaginary parts of the refractive index, respectively, and λ is the wavelength.

[7] The optical depth τ_λ of entire aerosol column can be calculated from the vertical profile $\sigma_\lambda(z)$,

$$\tau_\lambda = \int_0^{z_\infty} \sigma_\lambda(z) dz, \tag{3}$$

where z_∞ is the top of the atmosphere.

[8] From (1) and (3), one can obtain

$$\tau_\lambda = \int_{a_{\min}}^{a_{\max}} f(a) K_{e,\lambda}(a) da, \tag{4}$$

where $f(a)$ represents the columnar aerosol size distribution (with units, say, of $\mathrm{cm}^{-2}\mu\mathrm{m}^{-1}$),

$$f(a) = \int_0^{z_\infty} \varphi(z,a) dz. \tag{5}$$

[9] Equation (4) forms the basis for retrievals of $f(a)$ from a set of τ_λ [e.g., *King et al.*, 1978]. Since the weighting function $K_{e,\lambda}(a)$ is known (for given refractive index), the size distribution function $f(a)$ can be recovered by using equation (4) and spectral measurements of τ_λ. To derive the shape of $f(a)$, one must use τ_λ observations for a large number of wavelengths (e.g., 10 or more values of τ_λ). However, ozone and water vapor can absorb significantly for some of these wavelengths, requiring additional measurements to find the true aerosol optical thicknesses.

[10] In principal, two different wavelengths can be used for $f(a)$ retrievals, and these wavelengths can be chosen to avoid ozone and water vapor contamination. However, when using only two wavelengths, one has to assume a shape for the size distribution; then, given τ_λ at the two wavelengths, one can derive two parameters that describe the distribution. For example, the Junge power law has been used to model the aerosol size distribution [e.g., *Junge*, 1955; *Liou*, 2002]. This distribution has two parameters, the first of which is a scaling factor that is proportional to the aerosol concentration, while the second parameter represents a shaping constant that defines the slope of the Junge power law. These two parameters can be derived analytically from two values of τ_λ. This simple approach provides useful qualitative information about $f(a)$, but the spectral dependence of τ_λ predicted by the power law size distribution is often different from the observed one.

[11] We propose here another approach for $f(a)$ retrievals by using two wavelengths. We again must assume the shape of the size distribution; however, the shape of the assumed distribution is different from the Junge power law and is thought to be a more realistic representation of aerosol size distribution shapes. We assume that the shape of a normalized aerosol size distribution $\varphi^*(a)$,

$$\varphi^*(a) = \frac{1}{z_\infty} \int_0^{z_\infty} \varphi(z,a) dz, \tag{6a}$$

can be described by a combination of three lognormal distributions [*Hobbs et al.*, 1993]. These three distributions (modes) represent small, large, and giant particles. The parameters of such three-modal (combined) distributions are then specified to represent different types of tropospheric aerosols (see Table 1 for details).

[12] From (5) and (6a) it follows that

$$f(a) = \varphi^*(a) z_\infty. \tag{6b}$$

Note that z_∞ can be considered as a scaling parameter, and its value is unknown. Since the specification of this value does not affect our $f(a)$ retrieval, we set z_∞ = 1 km. Below, we outline a simple way of adjusting the combined distribution $f(a)$ to the spectral observations of τ_λ.

[13] We adjust the assumed distribution so that the τ_λ values derived from this distribution match the spectral observations of τ_λ. Specifically, taking two observed spectral values of τ_λ, denoted as $\tau_{obs,\lambda}$ (λ = 1 and 2), we estimate two bulk parameters of the assumed size distribution: the total number of particles N and the mean particle radius R. These two parameters are the zeroth moment and first moment of the size distribution, respectively:

$$N = \int_{a_{\min}}^{a_{\max}} f(a) da \tag{7}$$

$$R = \frac{1}{N} \int_{a_{\min}}^{a_{\max}} a f(a) da. \tag{8}$$

Table 1. Parameters (n_i, R_i, log σ_i, i = 1,. . .,3) for Models of Aerosol Size Distributions Described by the Sum of Three Lognormal Functions[a]

	Polar	Background	Maritime	Continental	Dust	Rural	Urban
n_1	2.17(+1)	1.29(+2)	1.33(+2)	3.20(+3)	7.26(+2)	6.65(+3)	9.93(+4)
n_2	1.86(−1)	5.97(+1)	6.66(+1)	2.90(+3)	1.14(+3)	1.47(+2)	1.11(+3)
n_3	3.04(−4)	6.35(+1)	3.06(0)	3.00(−1)	1.78(−1)	1.99(+3)	3.64(+4)
R_1	6.89(−2)	3.60(−3)	3.90(−3)	1.00(−2)	1.00(−3)	7.39(−3)	6.51(−3)
R_2	3.75(−1)	1.27(−1)	1.33(−1)	5.80(−2)	1.88(−2)	2.69(−2)	7.14(−3)
R_3	4.29(0)	2.59(−1)	2.90(−1)	9.00(−1)	1.08(+1)	4.19(−2)	2.48(−2)
log σ_1	2.45(−1)	6.45(−1)	6.57(−1)	1.61(−1)	2.47(−1)	2.25(−1)	2.45(−1)
log σ_2	3.00(−1)	2.53(−1)	2.10(−1)	2.17(−1)	7.70(−1)	5.57(−1)	6.66(−1)
log σ_3	2.91(−1)	4.25(−1)	3.96(−1)	3.80(−1)	4.38(−1)	2.66(−1)	3.37(−1)

[a]From *Hobbs et al.* [1993]. Read 2.17(+1) as 2.17×10^1. Columns "Continental" and "Dust" represent the "remote continental" and "desert dust storm" models, respectively. Here R_i is the mean particle radius (μm), n_i is the integral of the ith normal function, and log σ_i is a measure of particle polydispersity.

Note that the combined size distribution $f(a)$ can be defined by three bulk parameters: N, R, and the width (or difference between $a_{\max}$ and $a_{\min}$). The latter is fixed for an assumed size distribution (shape). Therefore, we only adjust two bulk parameters (N and R) by using the two spectral observations of $\tau_{obs,\lambda}$. The sensitivity tests of the $f(a)$ retrieval to shapes of the aerosol size distributions are discussed in section 3.1. These distributions have different bulk parameters. We will not consider the individual effect of each parameter (e.g., the width of distribution) on our retrieval. Instead, we estimate their combined effect (section 3.1). These results show that the retrieval is not sensitive to the details of distributions; this is in harmony with previous results [e.g., *Hansen and Travis*, 1974; *Lacis et al.*, 1992; *McGraw et al.*, 1995, 1998]. Referring to the modeled optical thickness as $\tau_{\mathrm{mod},\lambda}$ (N, R) (here we explicitly note the dependence of $\tau_{\mathrm{mod},\lambda}$ on N and R), the matching procedure varies N and R in $f(a)$, until $\tau_{obs,\lambda}$ and $\tau_{\mathrm{mod},\lambda}$ are equal for each of the two wavelengths.

[14] This matching procedure amounts to a simple shifting of the size distribution in two orthogonal directions because the shape of $f(a)$ is fixed. The first transformation is a vertical shift (along the y axis) of $f(a)$ (Figure 1a). This vertical shift simply changes N, the total number of particles, while keeping the mean particle radius R, fixed. The second transformation is a horizontal shift (along the x axis) of $f(a)$ (Figure 1b). This horizontal shift simply changes R, the mean particle radius, while keeping the total number of particles, N, fixed.

[15] From (4) and (7) it follows that τ_λ is a monotonically increasing function of N (for the vertical shift of $f(a)$, R is fixed). Also, from (4) and (8) one can conclude that τ_λ grows as R increases (for the horizontal shift of $f(a)$, N is fixed). This growth is due to the weighting function $K_{e,\lambda}(a)$. The horizontal shift tends to increase both the mean geometric cross-sectional area of the distribution (πa^2) and the mean extinction efficiency (Q_e). The latter is attributed to the reddening phenomenon [e.g., *Bohren and Huffman*, 1998; *Stephens*, 1994]. Figure 2 shows an example of the complex relationship between τ_λ and two parameters (N and R).

[16] Once the shape of the size distribution is decided, finding values of N and R is a simple matter. We assume that both the real and imaginary parts of the refractive index are known, and given the two inputs, the observed optical depths $\tau_{obs,\lambda}$ at two wavelengths, we have two equations and two unknowns (N and R). These can be solved for $\tilde{N}$ and $\tilde{R}$, the values of N and R, such that $\tau_{\mathrm{mod},\lambda}(\tilde{N}, \tilde{R})$ is equal to $\tau_{obs,\lambda}$ for both wavelengths. Here and below we denote the retrieved values by the tilde.

[17] In practice, the above description is lacking because we do not know in advance either the shape of the aerosol size distribution or the refractive index. However, one can make a reasonable assumption about the aerosol type (e.g., urban, or desert dust) and select an appropriate aerosol model (shape) for a particular case [e.g., *Hobbs et al.*, 1993]. Such selection should be performed by analysis of possible aerosol sources (e.g., their location, strength) and local meteorology (e.g., wind direction). Different kinds of the tropospheric aerosols have different values of the real refractive index n, but, for a given aerosol type, these n values do not vary much [e.g., *Dubovik et al.*, 2002]. Therefore one can set a plausible value of the real refractive index (e.g., urban aerosol). In contrast to n, the imaginary part of refractive index, m, varies through a large range,

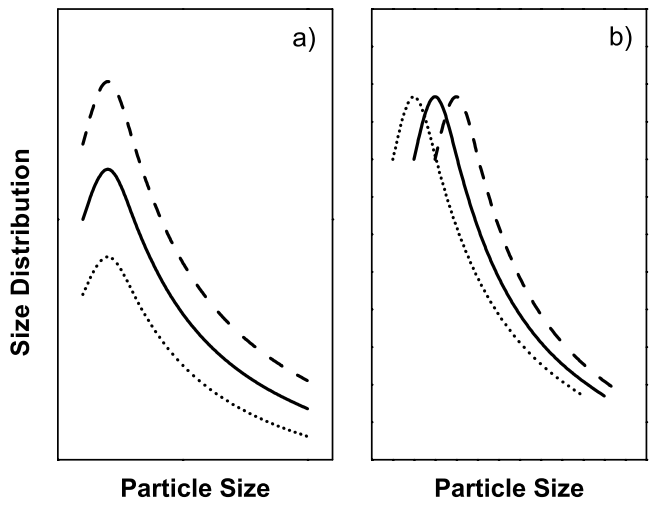

Figure 1. A schematic illustration of (a) the vertical shifting (along y-direction) and (b) horizontal shifting (along x-direction) of the size distribution function. The vertical shifting of size distribution changes the total number of particles, but does not change the mean particle radius. The opposite is true for the horizontal shifting of the size distribution.

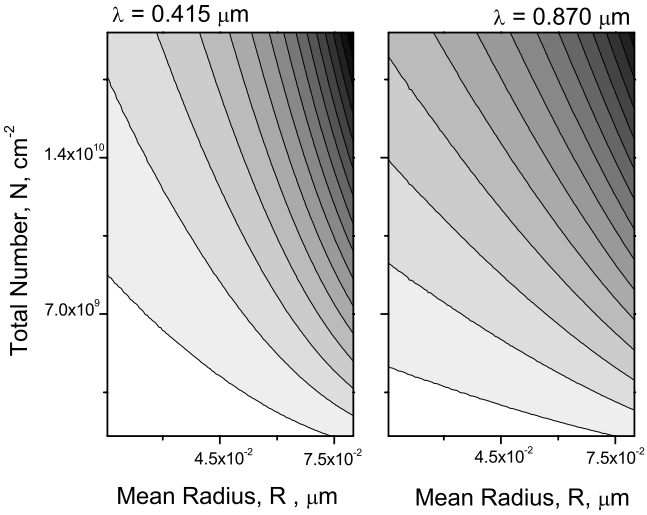

Figure 2. Two-dimensional diagrams of model optical depth τ_λ in terms of the total number N of particles and their mean radius R for two wavelengths (0.415 μm and 0.870 μm). These diagrams are obtained from Mie calculations for urban aerosol model [*Hobbs et al.*, 1993] and a given refractive index ($n = 1.5$ and $m = 0$). Dark and white colors represent high and low values of τ_λ, respectively.

up to several orders of magnitude. Therefore this parameter cannot be assumed and must be determined from observations. We now have three unknowns to determine (m, N, and R).

[18] In order to provide a third observational constraint, we include observations of the spectral diffuse irradiance ($D_{obs,1}$). To reduce the effect of ozone and water vapor contamination, we select wavelengths where ozone and water vapor absorb very weakly or not at all (e.g., $\lambda_1 = 0.415$ μm and $\lambda_2 = 0.870$ μm), and to reduce the effect of surface albedo on the diffuse irradiance, we select a wavelength where the surface albedo is small (e.g., $\lambda_1 = 0.415$ μm, for surfaces free of snow and ice). Our retrieval now requires three assumptions: (1) the shape of aerosol size distribution, (2) the real part of the refractive index n, and (3) the surface albedo $A_{s,1}$ at wavelength λ_1. Given these assumptions, we now have a closed problem of three inputs, and three unknowns.

[19] The three unknowns, $\tilde{m}$, $\tilde{N}$ and $\tilde{R}$, can be determined using iteration. We start with some initial ($i = 0$) value of the imaginary part $m^{(0)}$. The solution ($\tilde{m}$, $\tilde{N}$ and $\tilde{R}$) is not sensitive to the initial guess of the imaginary refractive index. However, the initial value, $m^{(0)}$, can affect the number of iterations. For this $m^{(0)}$ we find $N^{(0)}$ and $R^{(0)}$. The output of the first step is the derived aerosol size distribution function $f^{(0)}(a)$ with two parameters $N^{(0)}$ and $R^{(0)}$. The second step involves the following sequence: (1) calculation of the aerosol optical properties ($\tau^{(i)}_{\mathrm{mod},1}$, $\varpi^{(i)}_{\mathrm{mod},1}$ and $g^{(i)}_{\mathrm{mod},1}$) from Mie theory as a function of the imaginary refractive index m for the determined $f^{(i)}(a)$); (2) calculation of the modeled diffuse irradiance $D^{(i)}_{\mathrm{mod},1}$ as a function of m; (3) calculation of the difference $\delta^{(i)}_1 = |D_{obs,1} - D^{(i)}_{\mathrm{mod},1}|^2$ as a function of m; (4) obtainment of $m^{(i+1)}$ (where $\delta^{(i)}_1$ reaches its minimum). With regard to this last step, we performed calculations of diffuse irradiance for different type of aerosols, surface albedo values, and solar zenith angles; our calculations indicate that m is sharply defined and that the iteration is therefore very robust. We stop the iterations if the relative difference between $m^{(i+1)}$ and $m^{(i)}$ is less than or equal to 5%.

3. Sensitivity of Retrieval to Assumptions

[20] To estimate the sensitivity of the retrieval to the assumptions required for the retrieval, we performed an array of numerical tests. These tests follow the usual approach: We assume aerosol properties ($f(a)$, real and imaginary refractive indices, and the surface albedo), and using these quantities, we simulate "observations" (i.e., surface irradiances). We then perturb one of the inputs, for example the surface albedo, and using the simulated observations, we retrieve the parameters $\tilde{N}$, $\tilde{R}$, and $\tilde{m}$. The difference between retrieved $\tilde{N}$, $\tilde{R}$, and $\tilde{m}$ and the original values N^*, R^*, and m^* reveals the sensitivity of these values to changes the parameter in question (e.g., the surface albedo). For these tests, the original, true values are denoted by an asterisk. Radiative transfer calculations are performed using a Monte Carlo method for a solar zenith angle of 30° to find the simulated observations.

3.1. Numerical Tests

[21] Five numerical tests were performed to estimate the sensitivity of the retrieval results to the uncertainties in the two parameters that must be specified: the real part of the refractive index n and the surface albedo $A_{s,1}$. Table 2 shows the original values of n and $A_{s,1}$ that are used to simulate MFRSR observations and the assumed values of n and $A_{s,1}$ that are used in retrievals. Test A represents the most favorable case for retrieval: The original and assumed values are the same. Results of this test reveal the numerical accuracy of the retrieval. Tests B and C determine the sensitivity of the retrieval to assumed variations in n and $A_{s,1}$, respectively. To evaluate the accuracy of the retrieval, we use a percentage error,

$$\delta Q^{(i)} = 100\left|Q_{obs} - Q^{(i)}_{\mathrm{mod}}\right| / Q^{(i)}_{\mathrm{mod}}, \tag{9}$$

where Q denotes a parameter of interest (N, R, or m).

Table 2. Original and Assumed Values of Refractive Index (Real Part) n and Surface Albedo $A_{s,1}$ Which are Used in Numerical Experiments

	TestA		TestB_n14		TestB_n16		TestC_as00		TestC_as02	
	n	$A_{s,1}$	n	$A_{s,1}$	n	$A_{s,1}$	n	$A_{s,1}$	n	$A_{s,1}$
Original	1.5	0.1	1.4	0.1	1.6	0.1	1.5	0.0	1.5	0.2
Assumed	1.5	0.1	1.5	0.1	1.5	0.1	1.5	0.1	1.5	0.1

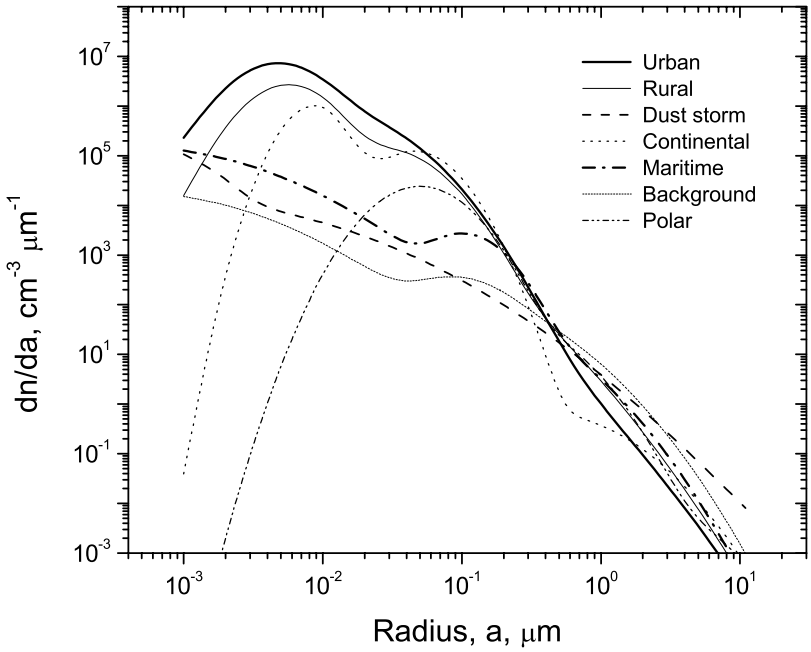

Figure 3. Model size distributions of selected atmospheric aerosols according to Table 1 [adapted from *Hobbs et al.*, 1993]. These distributions are normalized to produce the same aerosol optical depth 0.15 at a wavelength of 0.5 μm.

[22] We performed numerical experiments for the seven different models of aerosol size distribution shown in Table 1. These models produce aerosol optical depths τ_λ that vary over a broad range. For example, the difference between τ_λ calculated for the polar model and the dust storm model is about a factor of 100. To consider the effect of the size distribution shape only, we normalized these seven models in such a way as to provide the same optical thickness, 0.15, at 0.5 μm (Figure 3). This value represents roughly the globally and annually averaged value of the aerosol optical depth [e.g., *Ramanathan et al.*, 2001b]. For all models except the dust storm model, we obtained a similar accuracy for the retrieval results. However, for the dust storm model, the retrieval fails because the relative contribution of coarse particles (1 μm and larger) is significant, and as a result, τ_λ is almost spectrally independent. This failure means that this technique cannot be used for aerosols with a large value of R(1 μm and larger). One should be aware of substantial potential uncertainties in the aerosol retrieval when τ_λ shows weak spectral variability (e.g., ratio $\tau_2/\tau_1 > 0.5$, where $\lambda_1 = 0.415$ μm and $\lambda_2 = 0.870$ μm). Since we found that the accuracy of the retrieval is not sensitive to the shape of the aerosol size distribution function for all other cases, below we present results of the numerical tests that correspond to the urban aerosol model only. For all tests, we set $N^* = 137.0 \times 10^8$ cm^{-2}, $R^* = 3.4 \times 10^{-2}$ μm, and $m^* = 1.0 \times 10^{-2}$.

3.2. Microphysical Properties

[23] Table 3 shows the results of the model retrievals. The iterative scheme converges to the solution relatively quickly: two to three iterations allow one to achieve the required accuracy ($\varepsilon = 5\%$). If the assumed values are equal to the original ones (Test A), then all three parameters (N, R, and m) are derived precisely (Table 3). Small (~10%) differences between the original and assumed values of the refractive index n produce considerable (~25%) differences in the total number of particles N (Table 3). This can be explained as follows. The aerosol optical depth is proportional to N and the extinction efficiency Q_e. The latter is a complex (nonlinear) function of n. If the assumed value of n is larger than its original value, then the retrieved parameter $\tilde{N}$ underestimates N^* (Table 3). If the assumed value of n is smaller than its original value, then the opposite is true (Table 3). However, small (~10%) uncertainties in the real refractive index n affect only slightly the retrievals of other two parameters (R and m) (Table 3).

[24] Variations in surface albedo have no effect on the direct irradiances $S_{obs,1}$ and $S_{obs,2}$, but influence the diffuse irradiance $D_{obs,1}$. Variability of the value of m affects significantly the single scattering albedo of aerosol and, consequently, the diffuse irradiance. Therefore one can expect that uncertainties in $A_{s,1}$ will have a strong impact on the m retrievals only. Results of our numerical tests support this expectation (Table 3). Large (~100%) differences between the assumed value of $A_{s,1}$ and its original value produce considerable (~50–60%) differences in the retrieved value of m. If the assumed value of $A_{s,1}$ is larger than its original value, then the retrieved parameter $\tilde{m}$ overestimates m^* and vice versa (Table 3). However, the

Table 3. Relative Differences of the Microphysical (δm, δN, δR) Properties Obtained for Five Numerical Experiments[a]

	TestA	TestB_n14	TestB_n16	TestC_as00	TestC_as02
δm,%	1.4	−0.6	−0.1	−60.0	47.8
δN,%	−0.4	22.3	−27.7	3.3	−3.9
δR,%	0.9	−0.6	5.5	−2.6	2.7

[a]See Table 2.

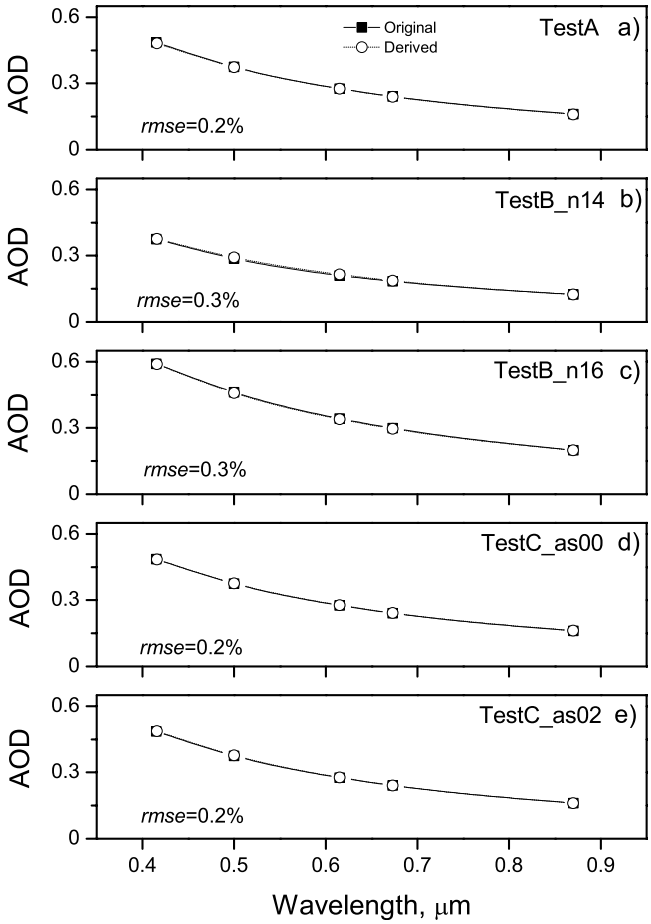

Figure 4. Aerosol optical depths (AOD) values that correspond to the original (square) and retrieved (circle) microphysical parameters of aerosol.

large (∼100%) uncertainties in the surface albedo $A_{s,1}$ affect only weakly the retrievals of the other two parameters (N and R). Fortunately, for non-snow-covered surfaces, the albedo $A_{s,1}$ is usually very small (∼0.05) at 0.415 μm and the retrieval is less sensitive to errors in albedo estimation for these small albedos (i.e., an error in albedo of ±0.02 at a true albedo of 0.05 has far less influence on the results than an error of ±0.2 at a true albedo of 0.5).

3.3. Optical Properties

[25] To estimate the sensitivity of optical parameters to the retrieval errors, we compare the optical properties (τ^*_λ, ω^*_λ, and g^*_λ) calculated for the original parameters (m^*, N^*, and R^*) with the optical properties ($\tilde{\tau}_\lambda$, $\tilde{\omega}_\lambda$, and $\tilde{g}_\lambda$) computed for the retrieved parameters ($\tilde{m}$, $\tilde{N}$, and $\tilde{R}$). The corresponding root-mean square errors (rmse) between original and retrieved values are shown (Figures 4, 5, and 6). These are defined as a square root of the sum $\frac{1}{k}\sum_{i=1}^{k}(f^*_i - \tilde{f}_i)^2$, where f is a given optical parameter and k is the number of wavelengths ($k = 5$). We start with the aerosol optical depth τ_λ (Figure 4). If the differences between all original and derived parameters are small, as in Test A above, then the τ^*_λ and $\tilde{\tau}_\lambda$ are in close agreement as well, as is evident in Figure 4. For experiment TestB_n14, the retrieved $\tilde{N}$ underestimates N^* considerably (∼25%), but τ^*_λ and $\tilde{\tau}_\lambda$ still agree well (Figure 4b). How can this be? The aerosol optical depth is a monotonically increasing function of both the total number N and the real part of the refractive index n (the weighting function $K_{e,\lambda}$ grows as n increases). Since in experiment ExpB_n14 the assumed value of n overestimates (by ∼10%) its original value (Table 2), this overestimation of n is compensated by the underestimation of N ($\tilde{N} < N^*$). A similar explanation can be applied to interpret the linkage among τ^*_λ and $\tilde{\tau}_\lambda$ for experiment TestB_n16 (Figure 4c).

[26] Let us consider the effect of the spectral surface albedo $A_{s,1}$ on τ_λ. A large (100%) overestimation of the assumed surface albedo $A_{s,1}$ increases substantially (∼50%) the retrieved $\tilde{m}$ and decreases slightly (∼3–4%) the derived $\tilde{N}$ (Table 3). The aerosol optical depth τ_λ is a monotonically increasing function of m (for size parameter $2\pi a/\lambda$ smaller than 4, the weighting function $K_{e,\lambda}$ grows as m increases) [e.g., *van de Hulst*, 1981]. Therefore overestimation of m compensates for the underestimation of N; thus τ^*_λ and $\tilde{\tau}_\lambda$ agree very closely (Figure 4d). In a similar way one can explain the good agreement between τ^*_λ and $\tilde{\tau}_\lambda$ for experiment TestC_as02 (Figure 4e). Overall, the uncertainties in the real part of refractive index n and the spectral albedo $A_{s,1}$ have a negligible impact on the retrieved aerosol optical depth $\tilde{\tau}_\lambda$. Since τ^*_λ and $\tilde{\tau}_\lambda$ are almost the same for all

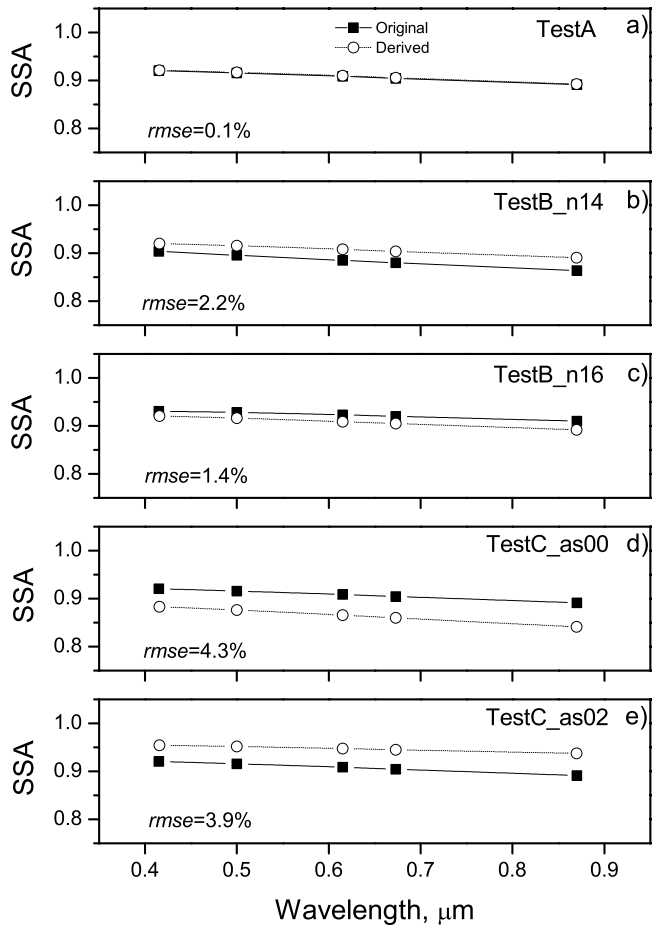

Figure 5. Aerosol single scattering albedo (SSA) values that correspond to the original (square) and retrieved (circle) microphysical parameters of aerosol.

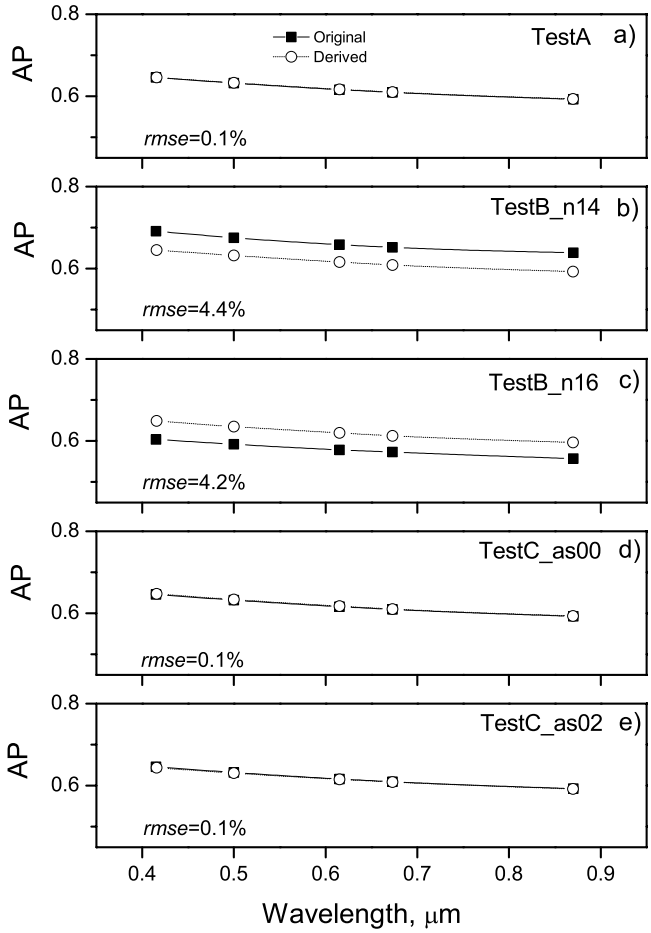

Figure 6. Asymmetry parameter (AP) values that correspond to the original (square) and retrieved (circle) microphysical parameters of aerosol.

considered experiments (Figure 4), the spectral values of direct irradiances S^*_λ and $\tilde{S}_\lambda$ agree very closely (not shown).

[27] In comparison with $\tilde{\tau}_\lambda$, the retrieved single-scattering albedo $\tilde{\omega}_\lambda$ is more sensitive to the assumed values of n and $A_{s,1}$ (Figures 4 and 5). For the entire aerosol atmospheric column, ω_λ can be written as

$$\omega_\lambda = \frac{\int_{a_{\min}}^{a_{\max}} f(a) K_{s,\lambda}(a) da}{\int_{a_{\min}}^{a_{\max}} f(a) K_{e,\lambda}(a) da}, \tag{10}$$

where the weighting function $K_{s,\lambda}(a)$ has a form

$$K_{s,\lambda}(a) = \pi a^2 Q_s(n, m; a/\lambda), \tag{11}$$

and Q_s is the scattering efficiency.

[28] From (10) it follows that ω_λ depends on $f(a)$ and two weighting functions $K_{e,\lambda}(a)$ and $K_{s,\lambda}(a)$. These functions have different spectral dependences of the complex refractive index (n and m) [e.g., *van de Hulst*, 1981, *Bohren and Huffman*, 1998], and these spectral dependences determine the sensitivity of $\tilde{\omega}_\lambda$ to the assumed values of n and $A_{s,1}$ (Table 2). Small (~10%) uncertainties in the assumed values of n influence weakly the retrieved single scattering albedo $\tilde{\omega}_\lambda$: At $\lambda = 0.415$ μm, the relative difference $|\delta\omega_\lambda|$ (between ω^*_λ and $\tilde{\omega}_\lambda$) is less then 2% (Figures 5b and 5c). Large (100%) uncertainties (from $A^*_{s,1} = 0.1$) in the assumed values of $A_{s,1}$ also influence weakly the retrieved single scattering albedo $\tilde{\omega}_\lambda$: At $\lambda = 0.415$ μm the relative difference $|\delta\omega_\lambda|$ is less then 4% (Figures 5d and 5e).

[29] The asymmetry factor g_λ is related to the phase scattering function P_λ by [e.g., *Liou*, 2002]

$$g_\lambda = \frac{1}{2} \int_{-1}^{1} P_\lambda(\mu)\mu \, d\mu. \tag{12}$$

The asymmetry factor lies in the range of $-1 \le g_\lambda \le 1$ and denotes how asymmetric the scattering of light is. For example, values of -1 and $+1$ imply that the incoming light is scattered only in the back and forward directions, respectively; while a value of 0 (e.g., Rayleigh scattering) means light is scattered into both hemispheres symmetrically. For a fixed size of particle, g_λ is a decreasing function of n (if size parameter $2\pi a/\lambda$ exceeds 1) [e.g., *Hansen and Travis*, 1974]. Figure 6 shows the spectral sensitivity of g_λ to changes in albedo and real part of the refractive index. The original value of n^* in TestB_n16 is larger than the original value of n^* in TestB_n14 (Table 2), and therefore the opposite is true for the original values of the asymmetry factor: g^*_λ (TestB_n16) is smaller than g^*_λ (TestB_n14) (Figures 6b and 6c). The retrieved values of $\tilde{g}_\lambda$ are almost the same for the numerical experiments considered here (Figure 6b and 6c).

[30] The diffuse irradiance D_λ is a function of both the aerosol optical properties (τ_λ, ω_λ, and g_λ) and the surface albedo $A_{s,\lambda}$. Although the original and retrieved values of the optical properties or surface albedo can be different, the retrieved diffuse irradiance $\tilde{D}_\lambda$ fits the original one D^*_λ very accurately (not shown) because in the retrieval, the microphysical/optical properties are forced to produce good agreement between $\tilde{D}_1$ and D^*_1 (section 2).

4. MFRSR Data Aerosol Retrieval

[31] Here we illustrate the performance of our technique by applying it to the MFRSR observations taken during 27 April 2003 in Mexico City, as part of the Mexico City Metropolitan Area (MCMA) field campaign (http://eaps.mit.edu/megacities/mcma_fieldcampaign/index.html). The environment in this region is urban, so we assume that the urban aerosol model (Table 1) is appropriate for our retrieval. Also, we assume n is equal to 1.4 [*Dubovik et al.*, 2002].

[32] *Castro et al.* [1997] have made measurements of the albedos of various surfaces in Mexico City. They report that in the UV spectral region ($\lambda \sim 0.4$ μm), the albedos for asphalted surfaces and gray cement surfaces are 0.05 and 0.1, respectively. *Michalsky et al.* [2003] have determined the albedo for vegetated surfaces at the Atmospheric Radiation Measurement Program's Southern Great Plains Site, and state that the albedo at 0.415 μm is in a range of 0.04 to 0.05, depending upon the type of vegetated surface. Given this information and the composite nature of the Mexico

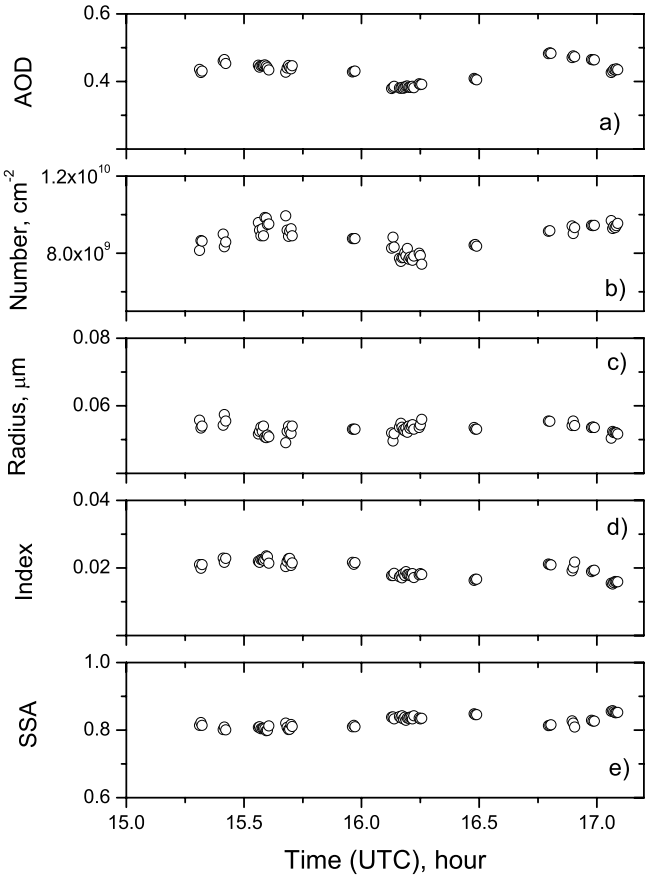

Figure 7. Time series of (a) aerosol optical depth, (b) the total number of particles, (c) the mean particle radius, (d) the imaginary part of refractive index, and (e) the single scattering albedo derived in Mexico City on 27 April 2003.

City surface (roads, buildings, some vegetation), we have estimated the surface albedo $A_{s,1}$ for the Mexico City area to be 0.07 at 0.415 μm. The sensitivity of the retrievals to the value specified for the surface albedo has been discussed in section 3. Small errors in our estimated value, say the true albedo is actually 0.05 instead of assumed 0.07, will cause an error of about 1% in the retrieved $\tilde{\omega}_\lambda$.

[33] *Michalsky et al.* [2001] discuss the accuracy of retrievals of aerosol optical thicknesses and associated irradiance measurements from the MFRSR. As stated in this paper, an MFRSR, calibrated using the Langley method, can produce transmissions that are accurate to about 1%. The transmission is defined as a ratio the measured irradiance at the surface to the top of atmosphere irradiance. The latter is determined from the Langley method. For the data presented in this paper, the MFRSR had been calibrated before, during, and after the field campaign, and we believe we have achieved the 1% accuracy goal in transmission. Because transmissions, rather than raw surface irradiance values, are used in the technique described here, we expect that the 1% will not unduly influence the retrievals described herein.

4.1. Example of Aerosol Retrievals

[34] For our retrievals, we used time periods that are hemispherically cloud free, which were found using the approach of *Long and Ackerman* [2000]. Figure 7a shows that this time period is characterized by substantial atmospheric aerosol loading, and the aerosol optical depth $\tau_{obs,1}$ (λ_1 = 0.415 μm), determined from the MFRSR measurements, changes slightly during a 2-hour period in the morning. The temporal variations of $\tau_{obs,1}$ and $\tilde{N}$ are strongly correlated (Figures 7a and 7b). The weak temporal variability of $\tilde{R}$ (Figure 7c) and $\tilde{m}$ (Figure 7d) suggest, not surprisingly, that the same type of aerosol persists during the considered time period.

[35] The retrieved size distribution function (with two bulk parameters $\tilde{N}$ and $\tilde{R}$) and the refractive index are used to calculate the single scattering albedo (Figure 7e) and the spectral behavior of the aerosol optical depth (Figure 8). Recall, we used only two spectral values of the aerosol optical depth $\tau_{obs,1}$ (λ_1 = 0.415 μm) and $\tau_{obs,2}$ (λ_2 = 0.870 μm). For these two wavelengths the model and observed values of the aerosol optical depth are the same (Figure 8). However, there is a small (~2%) difference between the model and observed values for other MFRSR wavelengths. Similarly good agreement is obtained for the whole considered period; the maximum difference is about 7% (at wavelength 0.673 μm). The corresponding spectral differences of the model $S_{\mathrm{mod},\lambda}$ and observed $S_{obs,\lambda}$ irradiances are 2 to 3 times smaller compared to differences of $\tau_{\mathrm{mod},\lambda}$ and $\tau_{obs,\lambda}$. In contrast to S_λ, D_λ depends on the surface albedo $A_{s,\lambda}$. The lack of precise information about $A_{s,\lambda}$ makes it impossible to provide a correct comparison of $D_{\mathrm{mod},\lambda}$ and $D_{obs,\lambda}$. However, good agreement between $D_{\mathrm{mod},\lambda}$ and $D_{obs,\lambda}$ can be obtained by changing $A_{s,\lambda}$ within reasonable limits.

[36] Surface spectrophotometric measurements in Mexico City [*Vasilyev et al.*, 1995] provided aerosol vertical column amount with a maximum value of 3×10^9 cm^{-2}. This value

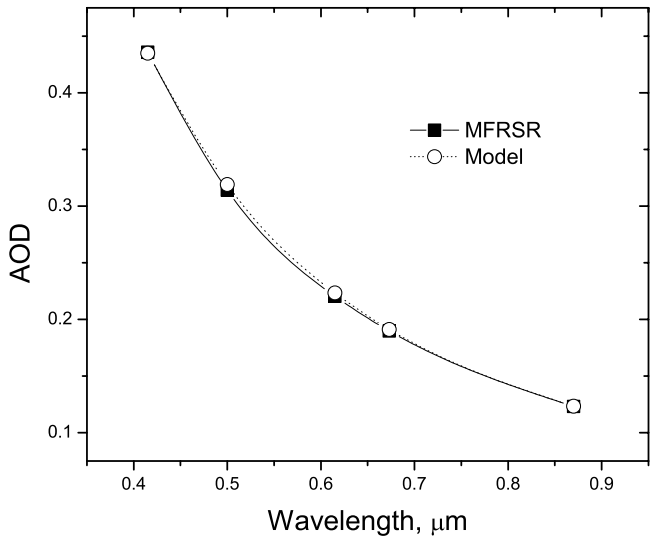

Figure 8. Example of the spectral dependence of the aerosol optical depth τ_λ (AOD): τ_λ derived from the MFRSR data (square) and τ_λ obtained from Lorenz-Mie calculations (circle) by using the derived aerosol size distribution and refractive index. The corresponding MFRSR measurements are taken in Mexico City on 27 April 2003 at 1531 UTC.

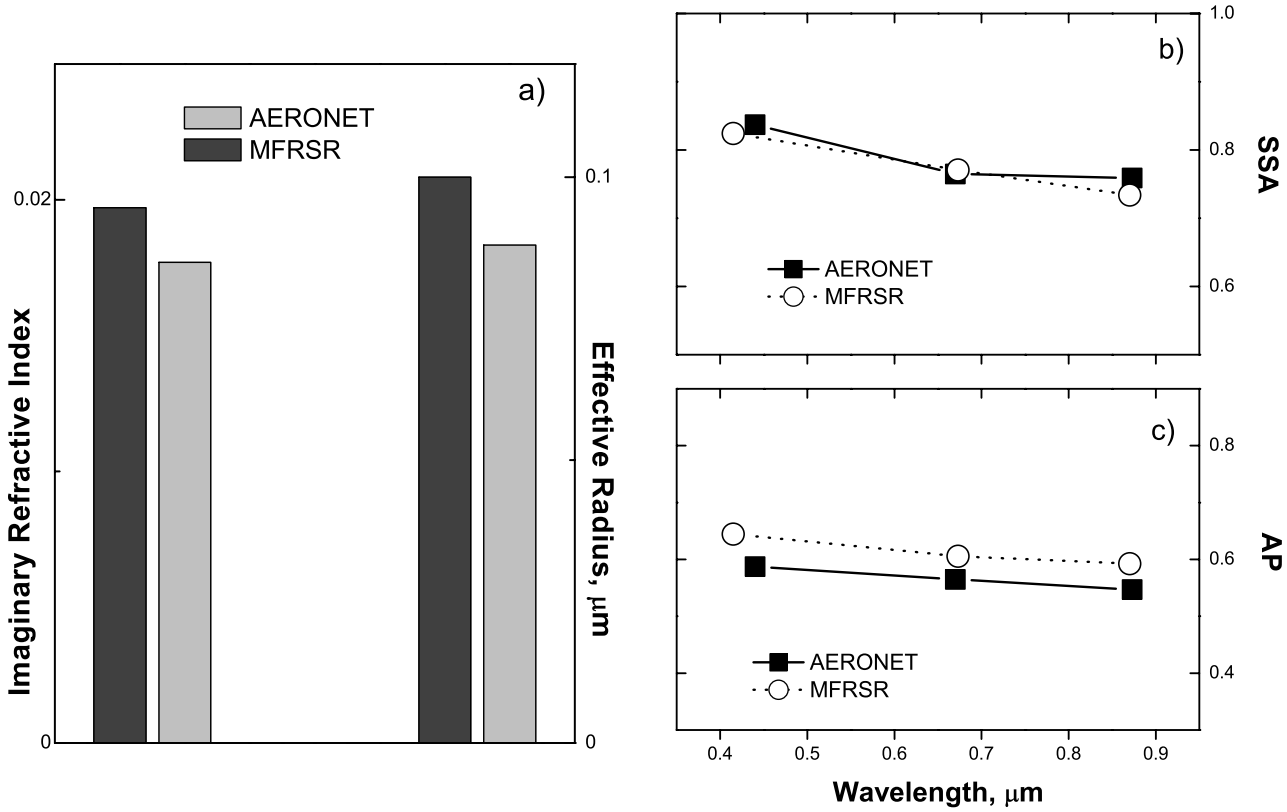

Figure 9. Aerosol properties derived from the MFRSR (black) and AERONET (shaded) data: (a) the imaginary refractive index (two left columns) for 0.415 μm (MFRSR) and 0.441 μm (AERONET), and the effective radius (two right columns); (b) the single scattering albedo; and (c) the asymmetry parameter.

was obtained for aerosol particles larger than 0.1 μm and is about 3 times lower than $\tilde{N}$ (Figure 7b). However, for Mexico City the contribution of small particles (less than 0.1 μm) to the aerosol vertical column amount is significant [e.g., *Castro et al.*, 1997; *Baumgardner et al.*, 2000], and $\tilde{N}$ includes this contribution. Therefore the difference between these two numbers can be attributed to this contribution. The mode of particle size distribution occurs at ~0.04 μm [*Baumgardner et al.*, 2000], and this value is comparable with $\tilde{R}$ (Figure 7c). Also, there is good agreement between $\tilde{\omega}_\lambda$ and the average value (0.8) of the single scattering albedo [*Raga et al.*, 2001]. Thus the retrieved aerosol parameters are in harmony with those of other investigators.

4.2. Comparison With AERONET Retrievals

[37] To further illustrate our retrievals, we compare MFRSR and AERONET retrievals of aerosol properties in Mexico City on 27 April 2003. Since these two instruments were not collocated (the separation between them was about 16 km), this comparison is not exact. These two instruments can be subject to different aerosol loadings as dictated by the local environmental situation and wind direction [e.g., *Doran et al.*, 1998] which causes pollution to be more pronounced over the AERONET site: The difference between aerosol optical depth derived from the AERONET and MFRSR data can exceed 40% (not shown). In contrast to the AERONET-derived aerosol optical depth, other AERONET products (e.g., the refractive index and size distribution) are obtained with coarse temporal resolution (varies from 0.3 hour to 1 hour): Additional time is required for sky scanning (solar almucantar during low sun and in the principal plane during high sun). Since MFRSR-retrievals are performed with high temporal resolution (20 s), we average them, and then the averaged values are compared with available AERONET data. For given temporal window (from 1520 UTC to 1720 UTC), there are available AERONET products obtained at 1636 UTC only (http://aeronet.gsfc.nasa.gov/photo_db/Mexico_City.html). We compare (Figure 9) these AERONET data (level 1.5) with 1-hour averaged MFRSR-retrievals (averaging from 1536 to 1636 UTC). Figure 9a indicates that the MFRSR-derived values of the imaginary refractive index and the effective radius differ slightly from the corresponding AERONET-derived values. As a result, the derived optical properties are slightly different as well (Figures 9b and 9c). The differences between the MFRSR-derived values and the AERONET-derived values (Figure 9) are small and within the uncertainties of the two retrieval techniques. For example, the retrieval error of the imaginary refractive index is about 5% for the MFRSR retrieval (section 3.1) and about 10% for AERONET retrieval [*Dubovik et al.*, 2000] in the most favorable error-free conditions (neither systematic nor random errors). However, in practice, this retrieval error can be substantially larger (~30–50%) [*Dubovik et al.*, 2002]. Furthermore, the suggested MFRSR retrieval assumes that the imaginary refractive index is the same for two consid-

ered wavelengths (λ_1 = 0.415 μm and λ_2 = 0.870 μm). In general, the wavelength dependence of the absorption of black carbon (the primary atmospheric absorber) can be relatively constant or variable (in the range from 0.3 μm and 1.0 μm) according to which kind of soot is examined [*Bergstrom et al.*, 2002]. To estimate the spectral dependence of the imaginary refractive index, we compare its AERONET-derived values at two wavelengths (0.441 μm and 0.873 μm): The difference between these two values is about 20%. The relatively weak spectral dependence may be responsible for some differences between the MFRSR and AERONET retrievals. Note that the AERONET-derived real refractive index is approximately equal to 1.43 and almost spectrally independent (we assume a value of 1.4). In addition, there may be small differences in the observed aerosol properties due to the physical separation of the two instruments, and we must note that the wavelengths used for MFRSR and AERONET retrievals (Figure 9a) are not exactly the same (0.415 μm and 0.441 μm, respectively).

[38] The MFRSR-derived products have some differences from the AERONET-derived ones:

[39] 1. MFRSR-retrieved microphysical properties and single scattering albedo have higher temporal resolution (~20 s) than those obtained from AERONET (from 0.3 to 1 hour as sky scanning requires).

[40] 2. MFRSR retrieval uses diffuse irradiance from hemispherical observations, whereas AERONET uses the sky radiances from solar almucantar during low sun and from the principal plane during high sun. In contrast to the AERONET sampling of diffuse radiation, the MFRSR sampling is independent of the solar zenith angle.

5. Discussion of the Retrieval Assumptions

[41] Our retrieval requires a few assumptions. In section 3, we estimated the sensitivity of the retrieval to uncertainties in the real refractive index and the surface albedo. Here we discuss the potential effects of other basic assumptions on the aerosol retrieval.

[42] We assume that aerosol particles are homogeneous spheres (section 2). This assumption could be appropriate for most of the non-dust-like aerosol particles that are either liquid or liquid coated. Dust-like particles have a complex irregular shape, a high sedimentation rate, and large sizes. For these particles, the spherical-nonspherical differences in the single-scattering properties, such as the total optical cross section, the single scattering albedo, and the asymmetry parameter are small [*Mishchenko et al.*, 1997]. Since the sedimentation rate of such particles is high and the particle shape effect on the single-scattering properties is weak, one can expect that dust-like particles do not change significantly the optical and radiative properties of tropospheric aerosol, except in very dusty conditions.

[43] The spectral independence of n is another assumption. In the retrieval, we assume that the two spectral values of n (at wavelengths λ_1 = 0.415 μm, λ_2 = 0.870 μm) are equal. In the visible and near-infrared wavelength ranges, the spectral variability of n is very weak for most tropospheric aerosols [e.g., *d'Almeida et al.*, 1991], and therefore this assumption can be considered reasonable.

[44] Also we assume that the shape of the size distribution (section 2) can be described as the sum of three lognormal distributions. Certainly, for some cases, this assumption may not be suitable. However, the single-scattering properties are not sensitive to the shape of the size distribution if two parameters (the effective radius and the effective variance) [e.g., *Hansen and Travis*, 1974; *Lacis et al.*, 1992], or a few lower-order moments [e.g., *McGraw et al.*, 1995, 1998] of the size distribution, are fixed. This means that the fine structure information of the size distribution (e.g., multimode versus single mode) is of very little importance. Since the direct and the diffuse irradiances are functions of the single-scattering properties, these radiative characteristics should not be very sensitive to the shape of the size distribution as well.

[45] The aerosol retrievals discussed here were performed for hemispherically cloud free periods, which is the optimal condition. Since this technique relies in part on the diffuse solar radiation scattered by aerosol, any diffuse scattering by clouds is a source of error and, for most cases, an unacceptably large error. Thus the usefulness of the approach is directly related to the amount of time that the sky is hemispherically cloud free. An analysis of about 9 years of data from the Southern Great Plains (SGP) site of the Atmospheric Radiation Measurement Program, which is located in Oklahoma, shows that significant periods of cloudless sky occur on approximately 30% of all days at the SGP. For this analysis, we define a "significant period" as at least 110 min of cloudless sky as determined by the algorithm of *Long and Ackerman* [2000]. Thus we will be able to use this new technique to determine aerosol properties for a period of about 2 hours or more on about one third of the days in the 9-year period. We expect the SGP numbers to be fairly typical of midlatitude sites.

[46] Applying the *Long and Ackerman* [2000] algorithm to data from the ARM site in Barrow Alaska produces a roughly comparable result. In this case, the sky is cloudless about 30% of the time that the sun is high enough above the horizon to allow the algorithm to work. The Barrow site is adjacent to the Arctic Ocean and so may be a bit more cloudy than other sites in the Arctic. Results from the two ARM tropical ocean sites show a much smaller incidence of cloudless sky owing to the ubiquitous fair weather cumulus. However, we expect that a tropical site such as Darwin Australia, which experiences a monsoon climate, should have fairly long stretches of time in the dry season during which aerosol loadings are high and the algorithm can be applied almost every day.

[47] There is no simple rule that determines a priori the amount of time that this new technique can be applied at an arbitrary location. However, the *Long and Ackerman* [2000] algorithm, which was developed for broadband solar radiometers, is easily adapted to use the broadband channel of the MFRSR (the MFRSR includes an "open" channel that measures the 0.3–1.0 μm total and diffuse SW, which can be used). Thus it provides a straightforward way to use the MFRSR data to determine how often and when the aerosol retrieval algorithm can be applied.

[48] We think that in practice, retrievals can be performed with some clouds in the sky as long as those clouds are low on the horizon and have only a very small contribution to the diffuse field. Additional numerical tests and comparison with field data will be carried out in the future to help address this issue.

[49] To the extent that the retrieved values are influenced by our assumptions, the retrieved microphysical properties of the aerosol can be considered as "effective" microphysical properties. These effective properties may be somewhat different from the true properties; however, the effective properties provide the same radiative characteristics (e.g., the direct and the diffuse irradiances) as the true properties, and in this regard, they are radiatively correct.

6. Summary

[50] Multifilter Rotating Shadowband Radiometers (MFRSRs) are widely deployed over the world. Currently, these radiometers provide routine observations of the spectral aerosol optical depth and single-scattering albedo. We propose here a simple retrieval technique that allows for simultaneous retrieval of the mean particle radius, total number of particles (for an assumed size distribution), and the imaginary refractive index from combined measurements of solar direct and diffuse irradiances. The technique consists of three steps that compose an iterative scheme. The first step obtains the aerosol size distribution from spectral measurements of direct irradiance (for a given refractive index). To reduce the effect of ozone and water vapor contamination, we use wavelengths where ozone and water vapor weakly affect the direct irradiance (λ_1 = 0.415 μm and λ_2 = 0.870 μm). The second step determines the imaginary part of refractive index from the diffuse irradiance for the aerosol size distribution determined during the first step. To reduce the effect of the surface albedo on the retrievals, we select a wavelength where the surface albedo is small (λ_1 = 0.415 μm) for surfaces not covered by snow or ice. The third step determines whether the iteration has converged.

[51] The sensitivity of the retrievals resulting from different aerosol types (shapes of the aerosol size distributions) and known uncertainty in the atmospheric aerosol model (real refractive index) and surface albedo has been analyzed. This analysis shows that successful retrievals of all aerosol characteristics can be achieved for the aerosols composed mainly of small and large (accumulation mode) particles. For example, small (~10%) uncertainties in the real refractive index and large (~100%) uncertainties in the surface albedo affect only slightly (~5%) the retrieval of the single scattering albedo (0.415 μm). If the relative contribution of coarse or giant particles (1 μm and larger) is significant, then the aerosol optical depth becomes almost spectrally independent, and the suggested technique fails to retrieve the aerosol properties.

[52] The technique has been successfully applied to derive temporal variations of aerosol microphysical properties derived from ground-based MFRSR measurements performed during one particular day (27 April 2003) in Mexico City. The MFRSR-derived aerosol properties are in good agreement with independent AERONET retrievals made also in Mexico City (27 April 2003). This favorable comparison suggests that a relatively inexpensive instrument, widely used over the world, can be applied to derive columnar aerosol optical and microphysical properties.

[53] To better understand the strengths and weaknesses of the technique, we plan to perform additional numerical experiments (e.g., different aerosol types and aerosol optical depths). We intend to assess the impact of clouds (e.g., different cloud fraction and cloud optical depth) and how this would limit the applicability of the retrieval. In addition, we will use available independent aircraft data and ground-based observations to further evaluate this method.

[54] **Acknowledgments.** This research was supported by the U.S. Department of Energy (DOE) under the auspices of the Atmospheric Science Program of the Office of Biological and Environmental Research, under contract DE-AC06-76RLO 1830 at the Pacific Northwest National Laboratory (PNNL). PNNL is operated for the U.S. DOE by Battelle Memorial Institute. We are grateful to C. Long and D. Flynn for assistance in analysis of broadband shortwave data and AERONET data, respectively. We thank two anonymous reviewers for thoughtful comments.

References

Alexandrov, M. D., A. A. Lacis, B. E. Carlson, and B. Cairns (2002), Remote sensing of atmospheric aerosols and trace gases by means of Multifilter Rotating Shadowband Radiometer: I. Retrieval algorithm, *J. Atmos. Sci.*, *59*, 524–543.

Baumgardner, D., G. B. Raga, G. Kok, J. Ogren, I. Rosas, A. Baez, and T. Novakov (2000), On the evolution of aerosol properties at a mountain site above Mexico City, *J. Geophys. Res.*, *105*, 22,243–22,253.

Bergstrom, R., P. Russell, and P. Hignett (2002), Wavelength dependence of the absorption of black carbon particles: Predictions and results from the TARFOX experiment and implications for the aerosol single scattering albedo, *J. Atmos. Sci.*, *59*, 567–577.

Bohren, C., and D. Huffman (1998), *Absorption and Scattering of Light by Small Particles*, 530 pp., John Wiley, Hoboken, N. J.

Castro, T., L. G. Ruiz-Suarez, J. C. Ruiz-Suarez, M. J. Molina, and M. Montero (1997), Sensitivity analysis of a UV radiation transfer model and experimental photolysis rates of NO_2 in the atmosphere of Mexico City, *J. Atmos. Environ.*, *31*, 609–620.

D'Almeida, G. A., P. Koepke, and E. P. Shettle (1991), *Atmospheric Aerosols: Global Climatology and Radiative Characteristics*, A. Deepak, Hampton, Va.

Doran, J. C., et al. (1998), The IMADA-AVER boundary layer experiment in the Mexico City area, *Bull. Am. Meteorol. Soc.*, *79*, 2497–2507.

Dubovik, O., et al. (2000), Accuracy assessments of aerosol optical properties retrieved from Aerosol Robotic Network (AERONET) Sun and sky radiance measurements, *J. Geophys. Res.*, *105*, 9791–9806.

Dubovik, O., et al. (2002), Variability of absorption and optical properties of key aerosol types observed in worldwide locations, *J. Atmos. Sci.*, *59*, 590–608.

Hansen, J. E., and L. D. Travis (1974), Light scattering in planetary atmospheres, *Space Sci. Rev.*, *16*, 527–610.

Harrison, L., and J. Michalsky (1994), Objective algorithms for the retrieval of optical depths from ground-based measurements, *J. Appl. Opt.*, *22*, 5126–5132.

Harrison, L., J. Michalsky, and J. Berndt (1994), Automated multifilter rotating shadow-band radiometer: an instrument for optical depth and radiation measurements, *Appl. Opt.*, *33*, 5118–5125.

Haywood, J., and O. Boucher (2000), Estimates of the direct and indirect radiative forcing due to tropospheric aerosols: A review, *Rev. Geophys.*, *38*, 513–543.

Haywood, J., D. Roberts, A. Slingo, J. Edwards, and K. Shine (1997), General circulation model calculations of the direct radiative forcing of tropospheric sulfate and fossil-fuel aerosol, *J. Clim.*, *10*, 1562–1577.

Hobbs, P., et al. (1993), *Aerosol-Cloud-Climate Interactions*, 233 pp., Elsevier, New York.

Holben, B., et al. (1998), A federated instrument network and data archive for aerosol characterization, *Remote Sens. Environ.*, *66*, 1–16.

Intergovernmental Panel on Climate Change (IPCC) (2001), *Climate Change 2001, The Scientific Basis*, edited by J. T. Houghton et al., 881 pp., Cambridge Univ. Press, New York.

Junge, C. (1955), The size distribution and aging of natural aerosol as determined from electrical and optical data on the atmosphere, *J. Meteorol.*, *12*, 13–25.

King, M., D. Byrne, B. Herman, and J. Reagan (1978), Aerosol size distribution obtained by inversion of spectral optical depth measurements, *J. Atmos. Sci.*, *35*, 2153–2167.

Lacis, A., J. E. Hansen, and M. Sato (1992), Climate forcing by stratospheric aerosols, *Geophys. Res. Lett.*, *19*, 1607–1610.

Liou, K. N. (2002), *An Introduction to Atmospheric Radiation*, 583 pp., Elsevier, New York.

Long, C. N., and T. P. Ackerman (2000), Identification of clear skies from broadband pyranometer measurements and calculation of downwelling shortwave cloud effects, *J. Geophys. Res.*, *105*, 15,609–15,626.

McGraw, R., P. I. Huang, and S. E. Schwartz (1995), Optical properties of atmospheric aerosols from moments of the particle size distribution, *Geophys. Res. Lett.*, *22*, 2929–2932.

McGraw, R., S. Nemesure, and S. E. Schwartz (1998), Properties and evolution of aerosols with size distributions having identical moments, *J. Aerosol Sci.*, *29*, 761–772.

Michalsky, J. J., J. A. Schlemmer, W. E. Berkheiser, J. L. Berndt, L. C. Harrison, N. S. Laulainen, N. R. Larson, and J. C. Barnard (2001), Multiyear measurements of aerosol optical depth in the Atmospheric Radiation Measurement and Quantitative Links programs, *J. Geophys. Res.*, *106*, 12,099–12,107.

Michalsky, J., Q. Min, J. Barnard, R. Marchand, and P. Pilewskie (2003), Simultaneous spectral albedo measurements near the Atmospheric Radiation Measurement Southern Great Plains (ARM SGP) central facility, *J. Geophys. Res.*, *108*(D8), 4254, doi:10.1029/2002JD002906.

Mishchenko, M., L. D. Travis, R. A. Kahn, and R. A. West (1997), Modeling phase functions for dustlike tropospheric aerosols using a shape mixture of randomly oriented polydispersed spheroids, *J. Geophys. Res.*, *102*, 16,831–16,847.

Petters, J. L., V. K. Saxena, J. R. Slusser, B. N. Wenny, and S. Madronich (2003), Aerosol single scattering albedo retrieved from measurements of surface UV irradiance and a radiative transfer model, *J. Geophys. Res.*, *108*(D9), 4288, doi:10.1029/2002JD002360.

Raga, G. B., T. Castro, and D. Baumgardner (2001), The impact of megacity pollution on local climate and implications for the regional environment: Mexico City, *J. Atmos. Environ.*, *35*, 1805–1811.

Ramanathan, V., et al. (2001a), Indian Ocean Experiment: An integrated analysis of the climate forcing and effects of the great indo-Asian haze, *J. Geophys. Res.*, *106*, 28,371–28,398.

Ramanathan, V., et al. (2001b), Aerosol, climate and the hydrological cycle, *Science*, *204*, 2119–2124.

Russell, P. B., P. V. Hobbs, and L. L. Stowe (1999), Aerosol properties and radiative effects in the United States east coast haze plume: An overview of the Tropospheric Aerosol Radiative Forcing Observational Experiment (TARFOX), *J. Geophys. Res.*, *104*, 2289–2307.

Stephens, G. (1994), *Remote Sensing of the Lower Atmosphere*, 523 pp., Oxford Univ. Press, New York.

van de Hulst, H. C. (1981), *Light Scattering by Small Particles*, 470 pp., Dover, Mineola, N. Y.

Vasilyev, O. B., et al. (1995), Spectral optical properties of the polluted atmosphere of Mexico City (spring-summer 1992), *J. Geophys. Res.*, *100*, 26,027–26,044.

Yu, H., et al. (2004), Direct radiative effect of aerosols as determined from a combination of MODIS retrievals and GOCART simulations, *J. Geophys. Res.*, *109*, D03206, doi:10.1029/2003JD003914.

T. P. Ackerman, J. C. Barnard, and E. I. Kassianov, Pacific Northwest National Laboratory, 902 Battelle Boulevard, P.O. Box 999, Richland, WA 99352, USA. (evgueni.kassianov@pnl.gov)